Wavelength-induced polarization bistability in 1550 nm VCSELs subject to orthogonal optical injection

M. S. Torre,[1] A. Quirce,[2,3] A. Valle,[2,*] and L. Pesquera[2]

[1]*Instituto de Física "Arroyo Seco," U.N.C.P.B.A., Pinto 399 (7000) Tandil, Argentina*
[2]*Instituto de Física de Cantabria, CSIC-Universidad de Cantabria, Avda. Los Castros s/n, E-39005 Santander, Spain*
[3]*Departamento de Física Moderna, Universidad de Cantabria, Avda. Los Castros s/n, E-39005 Santander, Spain*
**Corresponding author: valle@ifca.unican.es*

Received June 17, 2010; revised October 8, 2010; accepted October 11, 2010; posted October 11, 2010 (Doc. ID 130247); published November 8, 2010

We report on a theoretical and experimental investigation of the bistable behavior of the polarization of long-wavelength single-transverse mode vertical-cavity surface-emitting lasers (VCSELs) when subject to orthogonal optical injection. We have studied the bistability properties of the polarization switching that appear when changing the master laser wavelength with a fixed master laser power. Two bistable regions are found for polarization switchings appearing at short and long wavelengths. The directions of the obtained hysteresis cycles are in agreement with the experimental results. The widths of both bistable regions are also found to be similar and nearly independent of the injected power. The width of the region where polarization switching takes place is shown to increase as the injected power is increased. A good overall qualitative agreement is found between our theoretical and experimental results.

OCIS codes: 140.5960, 140.7260, 190.1450, 260.5430.

1. INTRODUCTION

Optical injection in semiconductor lasers is an attractive method to achieve bistable behavior in those devices [1]. Bistable laser diodes have applications in all-optical signal processing, optical switching, and optical storage [1–3]. The use of vertical-cavity surface-emitting laser diodes (VCSELs) in those applications has recently increased due to the unique characteristics of those devices like single-longitudinal mode operation, low threshold current, circular-beam profile, and the possibility to fabricate large two-dimensional arrays [3]. Also short-wavelength (SW, 850 nm) VCSELs are widely used in short haul optical communications and optical network interconnects, while long-wavelength (LW) VCSELs are attracting much interest for use as low cost sources in single-mode fiber metropolitan area [3–5]. Optical injection in VCSELs has also been used for improving the modulation characteristics of these devices without modifying their design. A significant reduction in the frequency chirp under modulation [4] and a large improvement of the laser intrinsic frequency response [5] have been obtained in single-mode VCSELs subject to optical injection.

Emission in different polarizations and transverse modes is usually found in free-running VCSELs [6]. While emission in several transverse modes is usually attributed to spatial hole burning effects, the polarization behavior can be influenced by different physical mechanisms. The light emitted by the VCSEL is usually linearly polarized along one of the two orthogonal directions in the plane of the active region. Polarization switching (PS) between both linearly polarized modes is often observed when the injection current or temperature is varied [7–11]. Optical injection strongly affects the polarization characteristics of VCSELs when linearly polarized light from a master laser (ML) source is injected orthogonally to the linear polarization of the free-running VCSEL. In this configuration, known as the "orthogonal optical injection," switching from the polarization of the solitary VCSEL to the orthogonal linear polarization has been observed as the injected power increases [12–27]. Optical bistability associated with the PS induced by orthogonal optical injection has also been observed in experimental [12–18,22–27] and in theoretical [19,20,24] works. "Intensity-induced polarization bistability" has been usually observed: the hysteresis was seen in the slave laser polarization when the intensity of the injection power was varied [12–20]. Less attention has been paid to the "wavelength-induced polarization bistability," which is the bistability found in the VCSEL when changing the ML wavelength with a fixed ML power. That bistability has been first found in experiments using 850 nm wavelength VCSELs [22,23]. It was shown that the change in the ML wavelength leads to two successive PSs in such a way that only the PS appearing in the longer wavelength regime exhibited bistable behavior [22,23]. In these experiments the excitation of another perpendicular polarized higher-order transverse mode played a relevant role. Theoretical work on a single-transverse mode VCSEL has shown that both PSs can exhibit bistable regions [24]. The

dependency of hysteresis widths on ML power has also been analyzed from experimental [22,23] and theoretical [24] points of view.

Recent experimental investigations [15,25–27] have shown that LW (1550 nm) single-transverse and polarization mode VCSELs also exhibit wavelength-induced polarization bistability when subject to orthogonal optical injection. Experiments with 1550 nm VCSELs seem interesting due to the potential of these devices for their use in optical interconnects, optical switching, and optical signal processing at that important telecommunication wavelength. As the ML wavelength λ_{ML} is scanned near the resonance wavelength of the depressed linearly polarized mode, and for a fixed injected power P_{inj}, the VCSEL exhibits two successive PSs. Bistable regions are found for both SW and LW PSs when the VCSEL is biased well above threshold [25]. When the VCSEL is biased slightly above threshold, bistability is only observed in the LW PS. Recent theoretical analysis showed that the transition from one LW bistable region to two bistable regions is obtained as the bias current is increased [24].

In this work we study the wavelength-induced polarization bistability observed under orthogonal optical injection from a theoretical and experimental point of view. We obtain a qualitative agreement with the experimental results of [25] by using the spin-flip model (SFM) [8,9] extended to account for orthogonal optical injection. Previous theoretical analysis [24] has considered VCSELs with a small birefringence (0.038 nm) that exhibit PS without optical injection when changing the injection current. In that study two bistable regions were obtained, but the behaviors of the SW and LW bistable regions were very different. In our work we choose values of the model parameters in such a way that the polarization of the free-running VCSEL remains stable over the whole bias current range like in the VCSEL studied in [25]. With our choice of parameters the birefringence is much larger than in [24] because the suppressed (orthogonal) polarization is shifted 0.48 nm to the LW side with respect to the dominant one (parallel), according to the experimental value [25]. In this work we also obtain new experimental results by using the same device of [25]. We have done these measurements in order to perform a better comparison with the theory. Our theoretical and experimental results show that two bistable regions are found for both SW and LW PSs. The directions of theoretical hysteresis cycles are in agreement with the experimental results. The widths of both bistable regions are also found to be similar and nearly independent of the injected power. Values similar to the experimental ones are obtained for the hysteresis widths. A good qualitative agreement is then found between our experimental and theoretical results.

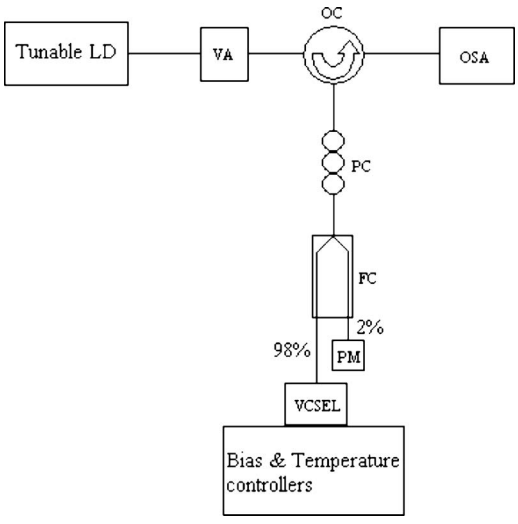

Fig. 1. Experimental setup for orthogonal optical injection in a VCSEL.

Our paper is organized as follows. In Section 2 we describe the experimental setup. In Section 3 we present the experimental results on the wavelength-induced polarization biestability. Section 4 is devoted to the description of the theoretical model. In Section 5 we present our theoretical results. Finally, in Section 6 discussion and summary are presented.

2. EXPERIMENTAL SETUP

Orthogonal optical injection is achieved by using the experimental setup presented in Fig. 1. This setup is based on the experiments of [25,26]. An all-fiber system has been developed in order to inject the light from a tunable laser (TL, Tunics Plus-CL) into a quantum-well commercial VCSEL (RayCan, Co.). Its bias current and temperature are controlled by a laser driver (Thorlabs LDC200) and a temperature controller (Thorlabs TED200), respectively. The VCSEL temperature was held constant at 297 K during the experiments. The output of the TL is injected into the VCSEL via a three-port polarization-maintaining optical circulator. Control of the optical power injected into the VCSEL is performed by using a variable attenuator (VA). A fiber coupler with a 98/2 split ratio and a power meter are used to measure the optical power arriving at the VCSEL, P_{inj}. The control of the polarization injected into the VCSEL is achieved by using a polarization controller. Spectral measurements are performed by using an optical spectrum analyzer (OSA) with 0.07 nm resolution. The spectrum measured at the OSA includes the power emitted by the VCSEL plus the reflection of the input light from the VCSEL cavity. The free-running VCSEL emits in the fundamental transverse mode with a threshold current of $I_{th}=1.62$ mA. The VCSEL emits in a linear polarization that we will call the "parallel" or y polarization, indistinctly. The emission in that polarization is stable, and no PS is observed for any bias above threshold. The second subsidiary mode has orthogonal (x) polarization and is shifted approximately 0.5 nm to the LW side of the lasing mode. Further details of this VCSEL, like the *L-I* characteristics and optical spectrum, can be found in [25].

3. EXPERIMENTAL RESULTS

Previous experimental papers on orthogonal optical injection in VCSELs have shown that as the wavelength of the TL, λ_{ML}, is scanned near the wavelength of the orthogonal linear polarization, λ_x, with fixed injected power P_{inj}, the VCSEL exhibits two successive PSs [15,21–23,25–27]. This is shown in the inset of Fig. 2 where the output

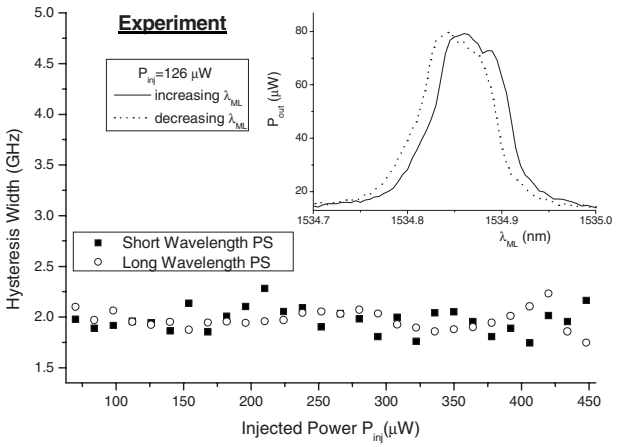

Fig. 2. Frequency widths of the bistable regions as a function of the injected power. Results corresponding to the SW and LW bistable regions are plotted with squares and circles, respectively. The inset shows the output power as a function of the wavelength of the injected light when $P_{\mathrm{inj}}=126\ \mu$W. Results corresponding to increasing and decreasing the wavelength are plotted with solid and dashed lines, respectively. In this figure $I_{\mathrm{VCSEL}}=4$ mA$=2.47I_{\mathrm{th}}$.

power in the x direction, P_{out}, as a function of λ_{ML} has been plotted with a solid line when λ_{ML} increases. When λ_{ML} is much smaller than the wavelength of the orthogonal mode ($\lambda_x=1534.81$ nm) the VCSEL is emitting in the y polarization, and the main contribution to P_{out} is given by the injected light reflected at the VCSEL. The increase in P_{out} as λ_{ML} increases while approaching λ_x indicates a first PS to the x-polarization, which we call SW PS. The subsequent decrease in P_{out} as λ_{ML} increases beyond λ_x shows that there is a second PS to the y polarization (LW PS). Both PSs are also clearly observed when measuring the output power in the y direction by using a circulator that does not maintain the polarization [15,26]. The inset of Fig. 2 also shows with a dotted line the evolution of P_{out} when λ_{ML} decreases. The behavior is similar to that already discussed but with a clear shift toward shorter wavelengths. The VCSEL then exhibits two successive PSs with two bistable regions in such a way that pure wavelength-induced polarization bistabilities are found like in [25]. Figure 2 shows the widths of both bistable regions measured as a function of the injected power when $I_{\mathrm{VCSEL}}=4$ mA (around $2.5I_{\mathrm{th}}$). Hysteresis widths fluctuate around a constant level of 2 GHz. The behavior of the hysteresis widths is similar for the SW and LW bistable regions. Figure 3 shows the width of the region where the PS takes place as a function of P_{inj} when $I_{\mathrm{VCSEL}}=4$ mA. The PS width increases as P_{inj} increases like in [25]. We have only considered the width obtained when increasing λ_{ML} because the results obtained when decreasing λ_{ML} are similar [10]. The widths of the bistable and PS regions have been calculated like in [25]. Also the same automatic control of the measurements described in [25] has been used to obtain Figs. 2 and 3.

4. MODEL

Our rate equation model for the optically injected VCSEL is based on the San Miguel–Feng–Moloney model, also called SFM [8,9]. The SFM model assumes a four-level

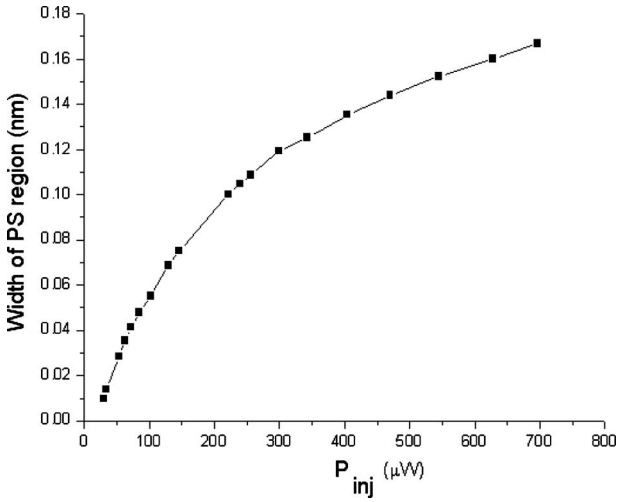

Fig. 3. Width of the PS region as a function of P_{inj} when $I_{\mathrm{VCSEL}}=4$ mA.

system in which electrons with different spins yield optical transitions with different circular polarizations of the light. We have used the extension of the SFM model included in [9] that accounts for the injection of an external field with an orthogonal polarization to that of the free-running VCSEL. In our simulation the parameters of the model are chosen such that the free-running VCSEL exhibits a stable and stationary y linearly polarized state. With our parameter choice the frequency of the y polarized mode is larger than the frequency of the x linear polarization ($\nu_y>\nu_x$) like in the experimental results. We therefore choose the optical injection along the x direction for obtaining PS from the y to the x linear polarizations. The rate equation model written in the frequency reference frame of the ML is given by

$$\frac{dE_x}{dt}=\kappa(1+i\alpha)(DE_x+idE_y-E_x)-i(\gamma_p+\Delta\omega)E_x-\gamma_aE_x+\kappa_{\mathrm{inj}}E_{\mathrm{inj}}+\sqrt{\beta_{sp}}\xi_x(t), \tag{1}$$

$$\frac{dE_y}{dt}=\kappa(1+i\alpha)(DE_y-idE_x-E_y)+i(\gamma_p-\Delta\omega)E_y+\gamma_aE_y+\sqrt{\beta_{sp}}\xi_y(t), \tag{2}$$

$$\frac{dD}{dt}=-\gamma_e[D(1+|E_x|^2+|E_y|^2)]+\gamma_e\mu-i\gamma_ed(E_yE_x^*-E_xE_y^*), \tag{3}$$

$$\frac{dd}{dt}=-\gamma_Sd-\gamma_ed(|E_x|^2+|E_y|^2)-i\gamma_eD(E_yE_x^*-E_xE_y^*), \tag{4}$$

where $E_{x,y}$ are the two linearly polarized slowly varying components of the field and D and d are two carriers variables. D accounts for the total population inversion between conduction and valence bands, while d is the difference between the population inversions for the spin-up and spin-down radiation channels. The internal VCSEL parameters are as follows: κ is the field decay rate, γ_e is the decay rate of D, γ_s is the spin-flip relaxation rate, α is

the linewidth enhancement factor, μ is the normalized injection current, γ_a is the linear dichroism, and γ_p is the linear birefringence. The fluctuating nature of the spontaneous emission is included in our model since $\xi_i(t)$ is a complex Gaussian term of zero mean and time correlation given by $\langle \xi_i(t)\xi_j(t')\rangle = 2\delta_{ij}\delta(t-t')$ and β_{sp} is the spontaneous emission rate.

The optical injection parameters are κ_{inj}, E_{inj}, and $\Delta\omega$, where κ_{inj} is the coupling coefficient, E_{inj} is the injected field amplitude, and $\Delta\omega$ is the detuning between the master and slave angular frequencies. We consider the case in which the coupling coefficient coincides with the field decay rate ($\kappa_{\text{inj}}=\kappa$) for the ideal case of an effectively mode-matched injected input beam [9]. The $\Delta\omega$ parameter is defined as the difference between the angular frequency of the injected light, ω_{inj}, and the reference angular frequency, ω_{ref}, intermediate between those of the x and y linear polarizations, i.e., $\Delta\omega=\omega_{\text{inj}}-\omega_{\text{ref}}$, where $\omega_{\text{ref}}=(\omega_x+\omega_y)/2$. The VCSEL parameters chosen for the simulations are $\gamma_e=1\ \text{ns}^{-1}$, $\gamma_p=192.1\ \text{ns}^{-1}$, $\gamma_a=1\ \text{ns}^{-1}$, $\gamma_s=1000\ \text{ns}^{-1}$, $\kappa=300\ \text{ns}^{-1}$, $\alpha=3$, and $\beta_{sp}=10^{-6}\ \text{ns}^{-1}$. With this parameter choice the free-running VCSEL emits in the y linear polarization and does not show PS in all the analyzed injected current ranges. Also a wavelength splitting between the two linear polarizations similar to the one experimentally measured is obtained. The scale of the injected power is taken to match the experimental minimum value of P_{inj} required to obtain PS induced by the orthogonal optical injection. In the experiment the minimum P_{inj} to achieve PS is 24 μW for a $2.6I_{\text{th}}$ bias current, while in our theoretical simulations the minimum E_{inj} required for PS at that current is 0.0384. Then in our calculations we consider that $P_{\text{inj}}=cE_{\text{inj}}^2$, where $c=1.628\times10^4\ \mu\text{W}$.

5. THEORETICAL RESULTS

In this section we will analyze the wavelength-induced polarization bistability obtained when changing λ_{ML} for a fixed P_{inj}. We show in Fig. 4(a) the output power corresponding to the x and y polarizations (I_x and I_y, respectively) as a function of the ML wavelength for fixed values of P_{inj} and I_{VCSEL}. We have considered the temporal variation of λ_{ML} illustrated in the inset of Fig. 4(a). λ_{ML} decreases from a value above the wavelength corresponding to the orthogonal mode [λ_x, shown in the inset of Fig. 4(a) with the upper horizontal line] until reaching an intermediate value between λ_x and λ_y (λ_y is also shown in that inset with the lower horizontal line). From that time a symmetric increasing dependence of λ_{ML} is considered. The variation of λ_{ML} is performed in discrete steps of height $\Delta\lambda$ and duration τ_{step} to approach the experimental conditions. The output power in both polarizations is averaged on the interval of time τ_{step} using a standard moving average. In Fig. 4(a) we show the results that correspond to decreasing λ_{ML}. As λ_{ML} decreases below 1534.90 nm I_x begins to increase in such a way that, when λ_{ML} is getting near the resonance wavelength of the orthogonal polarization of the VCSEL, all the power is transferred to the orthogonal polarization. This switching corresponds to the previously described LW PS in Fig. 2. As λ_{ML} decreases below the value λ_x, the output power I_x drops and

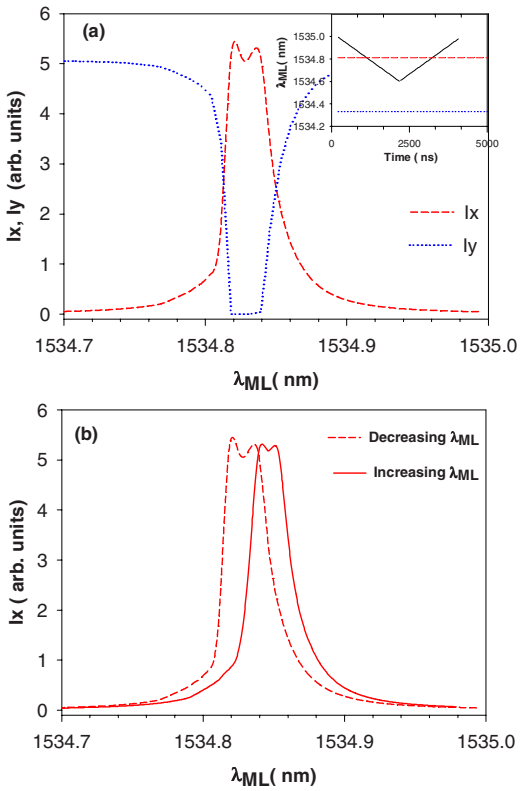

Fig. 4. (Color online) (a) Orthogonal (dashed line) and parallel (dotted line) polarization intensities, I_x, I_y, as functions of a decreasing ML wavelength, λ_{ML}. (b) Orthogonal polarization intensity, I_x, as a function of increasing (solid line) and decreasing (dashed line) ML wavelengths. In this figure $I=2.47I_{\text{th}}$, $P_{\text{inj}}=100\ \mu$W, $\Delta\lambda=0.007$ nm, and $\tau_{\text{step}}=35$ ns. The inset shows the considered temporal variation of λ_{ML}.

the total output power is transferred to the y polarization. Then there is a new PS that is similar to the SW PS shown in Fig. 2. Figure 4(b) shows the total output power in the orthogonal polarization as a function of λ_{ML} when decreasing and increasing λ_{ML}. The bistability behavior is shown clearly in this figure. The curve obtained when increasing λ_{ML} is shifted toward longer wavelengths in agreement with the experimental results shown in Fig. 2.

The results reported in Fig. 4(b) change when considering different values of the height of the steps, $\Delta\lambda$. We show in Fig. 5 the dependence of I_x on λ_{ML} when increasing and decreasing λ_{ML} for different values of $\Delta\lambda$. We find that the hysteresis width diminishes when $\Delta\lambda$ decreases. This result is in agreement with our experimental results when using different values of $\Delta\lambda$. For very small $\Delta\lambda$ (smaller than the values shown in Fig. 5), that is, modeling the variation of λ_{ML} in a continuous form, the positions of the maximum of I_x for increasing and decreasing λ_{ML} are exchanged. Then the direction of the hysteresis cycles is inverted in agreement with the results reported in [24].

We now analyze the theoretical dependence of the width of the PS region on the injected power. The width of the PS region is calculated by using the I_x versus λ_{ML} curves. This width is calculated by averaging over five values obtained around a level at 50% of the maximum value of I_x. This kind of average was also used in [25] to minimize the effect of some experimental fluctuations ob-

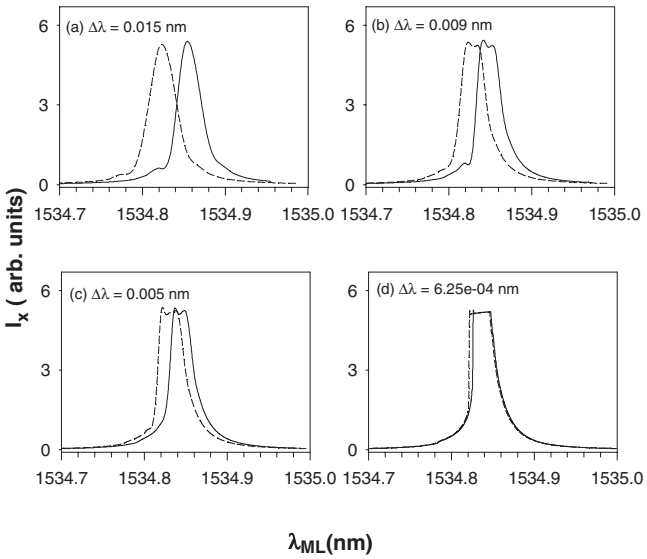

Fig. 5. Orthogonal polarization intensity, I_x, as a function of the ML wavelength when decreasing (dashed line) and increasing (solid line) λ_{ML} for different $\Delta\lambda$ values: (a) $\Delta\lambda=0.015$ nm, (b) $\Delta\lambda=0.009$ nm, (c) $\Delta\lambda=0.005$ nm, (d) $\Delta\lambda=6.25\times10^{-4}$ nm.

tained in the PS zones of the I_x versus λ_{ML} curves. In Fig. 6(a) we show the width of the regions where the PS to the orthogonal polarization takes place as a function of the injected power when $I_{VCSEL}=2.85I_{th}$. Results for decreasing

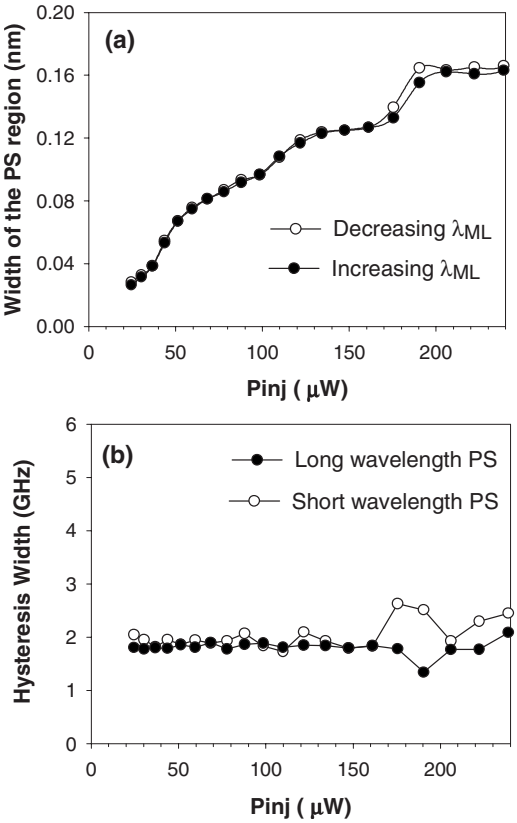

Fig. 6. (a) Widths of the PS regions as a function of the injected power for decreasing (white circles) and increasing (black circles) λ_{ML}. (b) Hysteresis width of the bistable regions as a function of the injected power. Results correspond to the LW (black circles) and SW (white circles) bistable regions. In both cases $I_{VCSEL}=2.58I_{th}$, $\Delta\lambda=0.007$ nm, and $\tau_{step}=35$ ns.

and increasing λ_{ML} are shown with open and filled circles, respectively. Similar widths are obtained when increasing and decreasing the ML wavelength in agreement with [25]. The PS width increases as P_{inj} increases in agreement with the results reported in Fig. 3. We have also found that the width of the PS region does not change for different values of $\Delta\lambda$. In Fig. 6(b) we show the width of both bistable regions as a function of the injected power P_{inj} when $I_{VCSEL}=2.85I_{th}$, and λ_{ML} is varied in 50 steps with $\Delta\lambda=0.007$ nm and $\tau_{step}=35$ ns. The value of $\Delta\lambda$ is near the experimental one (0.005 nm), while the theoretical duration of the pulse is much smaller than the experimental one (several seconds). The theoretical value of $\Delta\lambda$ has been chosen to get the best agreement with the experimental results of Fig. 2 for the hysteresis width. The theoretical value of τ_{step} has been chosen as long as possible while maintaining a reasonable computing time. The results reported in Fig. 6(b) show that the hysteresis widths of both bistable regions are similar and are nearly independent of the injected power, in agreement with Fig. 2. Also the directions of the hysteresis cycles are in agreement with the experimental results contained in Section 3 and in [25].

6. DISCUSSION AND CONCLUSIONS

There is a difference between our experimental results on the wavelength-induced polarization bistability and those presented in [25]. We have found that the width of both bistable regions does not depend on the injected power. However a step-like dependence was measured in [25] with a value of the injected power at the transition point that was independent of the VCSEL current. The previous transition occurred when the power emitted by the TL, P_{ML}, was around 0.8 mW. The reason for the step-like dependence is that 0.8 mW is the limit power in our TL for the operation of the active cavity control for mode-hop free (if $P_{ML}>0.8$ mW our TL operates without mode-hopping). In [25] changes in the injected power were obtained by changing P_{ML} in the TL. In our experiment those changes have been performed by using a VA after the TL and by choosing P_{ML} always larger than 0.8 mW to avoid the problem of switching between the two different operation modes (with or without mode-hop control) of the TL. In [25] power-induced polarization bistability was found near that transition value. We have repeated the measurements of [25] in our setup. No hysteresis cycles were observed when increasing P_{ML} (always above 0.8 mW) in a factor equal to the attenuation factor in our VA (in order to have the same injected power in the VCSEL as in [25]). Therefore the origin of the abrupt transition in the width of bistable regions and of the power-induced bistability found near $P_{ML}=0.8$ mW [25] lies in the internal operation of the TL and cannot be attributed to the internal VCSEL dynamics. We note however that different forms of polarization bistability with very wide power-induced hysteresis cycles can be observed by using our setup with P_{ML} always larger than the previous transition value [28].

The spontaneous emission rate chosen in our simulations is quite small. Spontaneous emission noise in this problem acts as a seed to trigger the dynamical evolution

that is basically deterministic above a low power level. We have checked that larger and more realistic values of the spontaneous emission rate (around $10^{-5}-10^{-4}$) do not change in a significant way our results.

We also note that the change in τ_{step} at a single wavelength step changes the hysteresis width. Experimental values of τ_{step} are of the order of several seconds. We cannot consider those values in the theory due to the prohibitive calculation times in the computer. Our approach to obtain the theoretical results has been the following. Given a wavelength step similar to the experimental one, we have then chosen a value of τ_{step} as long as possible while maintaining a reasonable computing time. This is the best strategy that we could devise in order to compare our theoretical and experimental results.

The locking region in Figs. 4 and 5 is more symmetric than those observed in [23,24]. Our solitary VCSEL emits in a linearly polarized single-transverse mode over the whole bias current range. Solitary VCSELs in [23,24] have different qualitative behaviors because emission in two transverse modes is found in [23], while a PS of the fundamental transverse mode was observed in [24]. This indicates that a possible reason for the symmetric locking region observed in our work could be the single mode behavior of our solitary device.

The main novelty of our simulations is the obtaining of constant hysteresis widths of the bistable regions [Fig. 6(b)] that are similar to our experimental results (Fig. 2). These results are qualitatively different to those obtained in [24] (Fig. 5 and 6) in which different maxima of the hysteresis widths are obtained for several values of the injected power. The theoretical models used in our work and in [24] are similar. Then the reason behind this different behavior is the consideration of very different device parameters in both works. The main difference in the values of the parameters corresponds to the birefringence value (our birefringence is 6.4 times larger than in [24]). Our birefringence value was large in order to obtain a theoretical wavelength splitting between the two linear polarizations similar to that measured in our device (0.5 nm).

The value of the spin-flip relaxation rate that we have used ($\gamma_s = 1000\ \text{ns}^{-1}$) is very large. We chose that value in order to have a stable polarization in the solitary laser because of the very large value of the birefringence parameter. An alternative that produces also a mono-stable behavior is the use of the SFM with a more realistic value of γ_s ($250\ \text{ns}^{-1}$) and a larger value of the linear anisotropy parameter ($\gamma_a = 2\ \text{ns}^{-1}$). Another alternative is the use of the simpler two-mode model with a single carrier density [29]. We intend to follow both alternatives in future work.

Summarizing, we have made a theoretical and experimental study of the PS that appears when 1550 nm VCSELs are subject to orthogonal optical injection. Our VCSELs are characterized by a large value of their birefringence parameter and by a linearly polarized emission along the whole current range. The wavelength-induced polarization bistability has been analyzed. We have found two bistable regions for PS appearing at SWs and LWs. We find that the widths of both bistable regions are similar and nearly independent of the injected power. The directions of the hysteresis cycles are in agreement with the experimental results. A good overall qualitative agreement has been found between the experimental and theoretical results when using typical values of the VCSEL parameters. A better agreement is expected if the working parameters of our VCSELs are extracted following the approach of [30].

ACKNOWLEDGMENTS

The authors would like to thank Dr. Antonio Hurtado and Professor Michael Adams from the University of Essex (UK) for fruitful discussions. The authors also thank the referees for constructive and clarifying comments. The authors acknowledge support from the Ministerio de Ciencia e Innovación (Spain) under the Project TEC2009-14581-C02-02. This work is also supported in part by CONICET Grant PIP 114-200801-00163, Argentina.

REFERENCES

1. H. Kawaguchi, "Bistable laser diodes and their applications: State of the art," IEEE J. Sel. Top. Quantum Electron. **3**, 1254–1270 (1997).
2. H. Kawaguchi, *Bistability and Nonlinearities in Laser Diodes* (Artech House, 1994).
3. F. Koyama, "Recent advances of VCSEL photonics," J. Lightwave Technol. **24**, 4502–4513 (2006).
4. C. H. Chang, L. Chrostowski, and C. J. Chang-Hasnain, "Injection locking of VCSELs," IEEE J. Sel. Top. Quantum Electron. **9**, 1386–1393 (2003).
5. L. Chrostowski, B. Faraji, W. Hofmann, M. C. Amann, S. Wieczorek, and W. W. Chow, "40 GHz bandwidth and 64 resonance frequency in injection-locked 1.55 μm VCSELs," IEEE J. Sel. Top. Quantum Electron. **13**, 1200–1208 (2007).
6. C. J. Chang-Hasnain, J. P. Harbison, G. Hasnain, A. C. von Lehmen, L. T. Florez, and N. G. Stoffel, "Dynamic, polarization and transverse mode characteristics of vertical cavity surface emitting lasers," IEEE J. Quantum Electron. **27**, 1402–1409 (1991).
7. K. D. Choquette, R. P. Schneider, K. L. Lear, and R. E. Leibenguth, "Gain-dependent polarization properties of vertical-cavity lasers," IEEE J. Sel. Top. Quantum Electron. **1**, 661–666 (1995).
8. M. San Miguel, Q. Feng, and J. V. Moloney, "Light-polarization dynamics in surface-emitting semiconductor lasers," Phys. Rev. A **52**, 1728–1739 (1995).
9. J. M. Martín-Regalado, F. Prati, M. San Miguel, and N. B. Abraham, "Polarization properties of vertical cavity surface-emitting lasers," IEEE J. Quantum Electron. **33**, 765–783 (1997).
10. A. Valle, L. Pesquera, and K. A. Shore, "Polarization behaviour of birefringent multitransverse mode vertical-cavity surface-emitting lasers," IEEE Photon. Technol. Lett. **9**, 557–559 (1997).
11. B. Ryvkin, K. Panajotov, A. Georgievski, J. Danckaert, M. Peeters, G. Verschaffelt, H. Thienpont, and I. Veretennicoff, "Effect of photon-energy-dependent loss and gain mechanisms on polarization switching in vertical-cavity surface-emitting lasers," J. Opt. Soc. Am. B **16**, 2106–2113 (1999).
12. Z. G. Pan, S. Jiang, M. Dagenais, R. A. Morgan, K. Kojima, M. T. Asom, and R. E. Leibenguth, "Optical injection induced polarization bistability in vertical-cavity surface-emitting lasers," Appl. Phys. Lett. **63**, 2999–3001 (1993).
13. J. B. Altes, I. Gatare, K. Panajotov, H. Thienpont, and M. Sciamanna, "Mapping of the dynamics induced by orthogonal optical injection in vertical-cavity surface-emitting laser," IEEE J. Quantum Electron. **42**, 198–207 (2006).
14. A. Hurtado, I. D. Henning, and M. J. Adams, "Two-wavelength switching with a 1550 nm VCSEL under single orthogonal optical injection," IEEE J. Sel. Top. Quantum Electron. **14**, 911–917 (2008).

15. A. Hurtado, I. D. Henning, and M. J. Adams, "Different forms of wavelength polarization switching and bistability in a 1.55 μm vertical-cavity surface-emitting laser under orthogonally polarized optical injection," Opt. Lett. **34**, 365–367 (2009).
16. B. S. Ryvkin, K. Panajotov, E. A. Avrutin, I. Veretennicoff, and H. Thienpont, "Optical-injection-induced polarization switching in polarization-bistable vertical-cavity surface-emitting lasers," J. Appl. Phys. **96**, 6002–6007 (2004).
17. I. Gatare, J. Buesa, H. Thienpont, K. Panajotov, and M. Sciamanna, "Polarization switching bistability and dynamics in vertical-cavity surface-emitting lasers under orthogonal optical injection," Opt. Quantum Electron. **38**, 429–443 (2006).
18. T. Mori, Y. Yamayoshi, and H. Kawaguchi, "Low-switching-energy and high-repetition-frequency all-optical flip-flop operations of a polarization bistable vertical-cavity surface-emitting laser," Appl. Phys. Lett. **88**, 101102 (2006).
19. M. Sciamanna and K. Panajotov, "Route to polarization switching induced by optical-injection in vertical-cavity surface-emitting lasers," Phys. Rev. A **73**, 023811 (2006).
20. I. Gatare, M. Sciamanna, M. Nizette, and K. Panajotov, "Bifurcation to polarization switching and locking in vertical-cavity surface-emitting lasers with optical injection," Phys. Rev. A **76**, 031803 (2007).
21. K. H. Jeong, K. H. Kim, S. H. Lee, M. H. Lee, B. S. Yoo, and K. A. Shore, "Optical injection-induced polarization switching dynamics in 1.5 μm wavelength single-mode vertical-cavity surface-emitting lasers," IEEE Photon. Technol. Lett. **20**, 779–781 (2008).
22. Y. Hong, K. A. Shore, A. Larsson, M. Ghisoni, and J. Halonen, "Pure frequency-polarisation bistability in vertical-cavity surface-emitting lasers subject to optical injection," Electron. Lett. **36**, 2019–2020 (2000).
23. Y. Hong, K. A. Shore, A. Larsson, M. Ghisoni, and J. Halonen, "Polarisation switching in a vertical-cavity surface-emitting semiconductor laser by frequency detuning," IEE Proc.: Optoelectron. **148**, 31–34 (2001).
24. I. Gatare, K. Panajotov, and M. Sciamanna, "Frequency-induced polarization bistability in vertical-cavity surface-emitting lasers with orthogonal optical injection," Phys. Rev. A **75**, 023804 (2007).
25. A. Valle, M. Gomez-Molina, and L. Pesquera, "Polarization bistability in 1550 nm wavelength single-mode VCSELs subject to orthogonal optical injection," IEEE J. Sel. Top. Quantum Electron. **14**, 895–902 (2008).
26. A. Quirce, A. Valle, and L. Pesquera, "Very wide hysteresis cycles in 1550-nm VCSELs subject to orthogonal optical injection," IEEE Photon. Technol. Lett. **21**, 1193–1195 (2009).
27. A. Hurtado, I. D. Henning, and M. J. Adams, "Wavelength polarization switching and bistability in a 1550-nm VCSEL subject to polarized optical injection," IEEE Photon. Technol. Lett. **21**, 1084–1086 (2009).
28. A. Hurtado, A. Quirce, A. Valle, L. Pesquera, and M. J. Adams, "Power and wavelength polarization bistability with very wide hysteresis cycles in a 1550 nm-VCSEL subject to orthogonal optical injection," Opt. Express **17**, 23637–23642 (2009).
29. J. Danckaert, B. Nagler, J. Albert, K. Panajotov, I. Veretennicoff, and T. Erneux, "Minimal rate equations describing polarization switching in vertical-cavity surface-emitting lasers," Opt. Commun. **201**, 129–137 (2002).
30. S. Barland, P. Spinicelli, G. Giacomelli, and F. Marin, "Measurement of the working parameters of an air-post vertical-cavity surface-emitting laser," IEEE J. Quantum Electron. **41**, 1235–1243 (2005).